UPDATES doi.org/10.1002/adsc.202300045 Advanced Synthesis & Catalysis

Mechanistic Insights into the Stepwise (4+2) Cycloaddition toward Chiral Fused Uracil Derivatives

Enrico Marcantonio,[a] Franca Zanardi,[a] Claudio Curti,[a,*] and Marco Lombardo[b,*]

[a] Department of Food and Drug, University of Parma, Parco Area delle Scienze 27 A, I-43124 Parma, Italy
E-mail: claudio.curti@unipr.it
[b] Department of Chemistry "Giacomo Ciamician" & Center for Chemical Catalysis (C3), University of Bologna, Via Selmi 2, I-40126 Bologna, Italy
E-mail: marco.lombardo@unibo.it

Manuscript received: January 15, 2023; Revised manuscript received: March 30, 2023;
Version of record online: April 28, 2023

Supporting information for this article is available on the WWW under https://doi.org/10.1002/adsc.202300045

Abstract: The mechanism of the previously reported stereoselective (4+2) cycloaddition of *N*-protected 6-methyluracil-5-carbaldehydes and (*E*)-*β*-nitrostyrenes catalyzed by Takemoto's tertiary amine/thiourea organocatalyst was explored, using density functional theory (DFT) calculations on a model representative reaction. The cyclization reaction, which afforded notable enantioenriched carbocycle-fused uracils embedding three contiguous stereocenters, was here proven to be the result of a four-step sequence comprising a key stereo-defining Michael addition, followed by a completely diastereoselective intramolecular Henry reaction. Going beyond the hitherto reported activation modes, a complex and unprecedented network of hydrogen-bonding interactions between the chiral catalyst and the reaction partners has been disclosed, in which the protonated tertiary amine and the thiourea moiety of the catalyst simultaneously activate both the electrophile and the nucleophile components. By applying the Energetic Span Model (ESM) to four competitive energetic profiles, we unveiled the most plausible reaction pathways best fitting the experimental data, with close correlation with the observed enantiomeric ratio of the product.

Keywords: Density functional calculations; Energetic Span Model; Fused-ring systems; Noncovalent interactions; Organocatalysis; Vinylogy

Introduction

Among the diverse synthetic strategies designed to achieve molecular complexity, asymmetric cascade reactions represent an ever-growing area of research that has found an incredible boost with the advent of asymmetric organocatalysis.[1] Inspired by Nature, the stability, safety, and versatility of chiral organocatalysts have made them perfectly suited to govern the stereochemical output of these transformations often producing chiral, enantiopure compounds embedding multiple stereocenters.[2]

An utmost important benefit of a one-pot organocascade process lies in the possibility of exploiting the intrinsic reactivity of high-energy synthetic intermediates, whose genesis and handling would be otherwise very challenging. This is the case of *ortho*-quinodimethane species of type **I** (*o*QDM, Scheme 1a), elusive yet highly reactive intermediates potentially accessible by *in-situ*, dearomative, vinylogous enolization of *ortho*-alkyl substituted aromatic carbaldehydes **II** or readily available derivatives thereof.[3]

Such compounds proved to be key intermediates in a variety of asymmetric organocascade processes, mainly (4+2) cycloadditions.[4] Of note, despite the large number of newly developed, asymmetric organocascades has allowed access to products of increasing structural complexity, a deep understanding of the catalytic cycles involved in such transformations has been largely overlooked. Regrettably, certification of the actual catalytic cycle(s) involved in an organocascade process by experimental observations is a difficult task, given the elusive nature of many intermediates rendering their identification quite

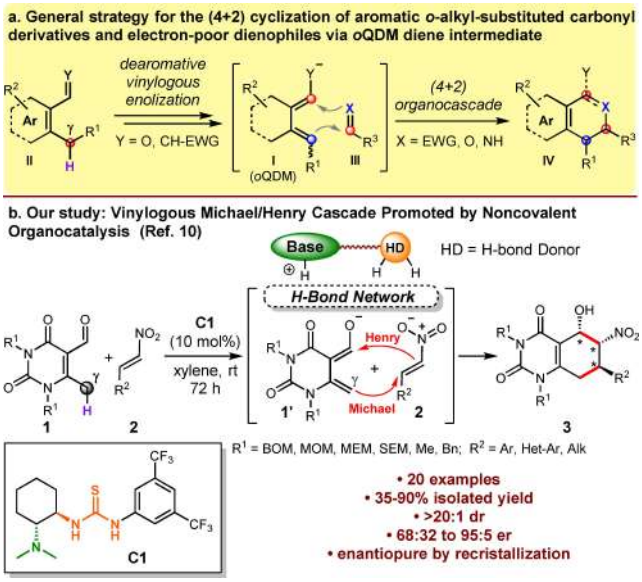

Scheme 1. (a) General strategy for the (4+2) cyclization via *o*QDM intemediates, and (b) our previously reported vinylogous, Michael/Henry cascade toward enantioenriched fused-uracil derivatives.

challenging.[5] To this end, quantum chemistry calculations, whose exploitation in organic chemistry has been considerably growing in recent years especially for the accuracy improvement of functionals in density functional theory (DFT), might come to help.[6]

Indeed, DFT analyses can considerably improve our understanding of the subtle mechanistic pathways and kinetic profiles featuring an organocatalytic cycle. A straightforward method to compare the efficiency (turnover frequency, TOF) of competing catalytic cycles based on DFT-computed energy profiles is represented by the Energetic Span Model (ESM), implemented by Kozuch et al. almost two decades ago.[7] Grounded on a paradigm shift stating that the efficiency of a catalytic transformation is not strictly dependent upon the nature of the rate-determining step, but instead by the difference between rate-limiting states, such as the so-called TOF-determining transition state (TDTS) and TOF-determining intermediate (TDI),[8] ESM has been successfully applied mainly to metal-catalyzed transformations, but in recent years examples have appeared in the literature also in organocatalytic transformations.[9] Our interest toward the development of enantioselective, vinylogous and organocatalytic transformations[2b] recently brought us to disclose a (4+2) cycloaddition between *N*-protected 6-methyluracil-5-carbaldehydes **1** and a series of nitroolefins **2**,[10] promoted by Takemoto's bifunctional tertiary amine-thiourea organocatalyst **C1** (Scheme 1b).[11] A series of chiral, fused uracil derivatives of type **3** embedding three contiguous stereocenters was efficiently accessed with excellent diastereocontrol and good enantioselectivities. In that occasion, a plausible catalytic cycle was proposed (Scheme 2), mainly based on the known ability of catalyst **C1** to noncovalently promote such reactions by weaving non-obvious H-bond networks with reagents and intermediates.[12]

Capitalizing on our precedents[13] we assumed that a "classical" Takemoto's mode of activation[11] was operative (mode A, Figure 2, *vide infra*), envisaging a four-step sequence which included: 1. a vinylogous dearomative enolization step, operated by the tertiary amine base of **C1** on uracil carbaldehyde **1** to afford the active *o*QDM species **1′**; 2. a stereo-defining, vinylogous Michael addition of **1′** on the *Re* face of nitroalkene **2** activated by the thiourea unit of **C1** by double hydrogen bonding; 3. a highly selective intramolecular Henry-type cyclization to secure formation of product **3**, (*Si*/*Re* approach), and 4. the final release of product **3** with concomitant decomplexation and recycling of the catalyst.

By following the reaction sequence proposed in Scheme 2, we herein report a detailed DFT mechanistic study and modelling of the entire catalytic cycle of a representative reaction, at the M06-2X/def2-TZVPP-IEFPCM (toluene)//M06-2X/6-31G(d)-IEFPCM (toluene) level of theory.[14] Furthermore, by applying Kozuk's ESM to the computed energetic profiles, we unveil the most plausible reaction pathway best fitting the experimental results, shedding light on the noncovalent activation modality operated by the catalyst.

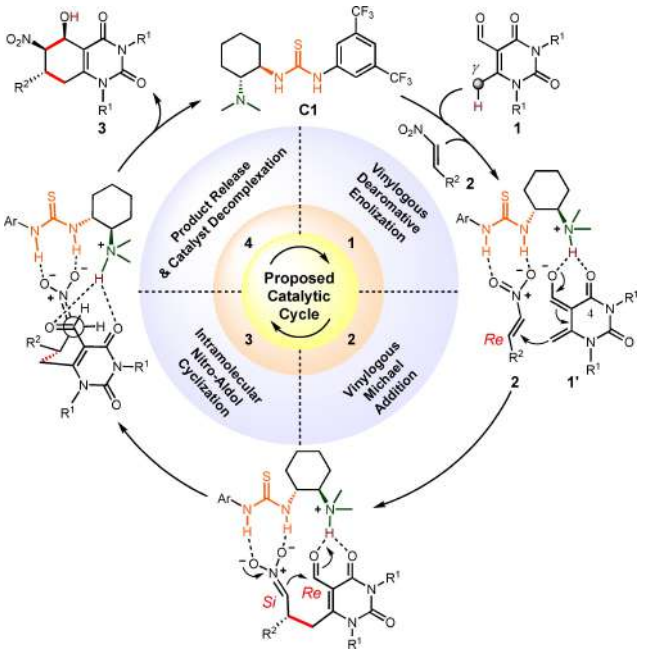

Scheme 2. Formerly Proposed Catalytic Cycle for the One Pot-Four Step (4+2) Cycloaddition between Uracil Derivatives **1** and Nitroalkenes **2**.[10]

Of note, while several DFT-based calculations have already been performed since the advent of enantioselective organocascade processes, they were zoomed to partial energetic profiles and re-stricted to key intermediates and transition states.[15] To the best of our knowledge, only rare studies on complete energy profiling of organocatalyzed reaction cascades have been reported so far,[16,9] whilst the application of ESM to get insights into the efficiency of a noncovalent organocatalyzed (4+2) cyclization is still unprecedented.

Results and Discussion

To fulfil the objectives of the work, we needed a model reaction featuring substrates with "computing-friendly" low-complexity structure with high probative output. We thus performed the reaction between *N*,*N*-dimethyl-protected 6-methyl-uracil-5-carbaldehyde **1a** (which had already proven to be a viable pronucleophile in our previous work)[10] and *trans*-*β*-nitrostyrene (**2a**) under the guidance of **C1** catalyst, affording the corresponding (5*S*,6*R*,7*R*)-configured fused uracil **3aa** in 50% yield and 68:32 enantiomeric ratio (*er*, Scheme 3).

Despite the non-brilliant results in terms of efficiency and enantioselectivity of this reaction as compared to the previously reported outcomes with more hindered *N*-BOM- or *N*-MOM-protected pronucleophiles, we considered it as a good reaction probe, willing to demonstrate the validity of our model in this intrinsically complex process with many competing kinetic pathways involved. The computational analysis of each step of the proposed sequence is reported in the following paragraphs.

1. Vinylogous, Dearomative Enolization Step. We first focused on the enolization step, implying deprotonation of 1a by the catalyst tertiary amine base, with the concomitant activation by complexation of the pronucleophile to the thiourea moiety of the bifunctional catalyst C1 (Figure 1a).[11,17]

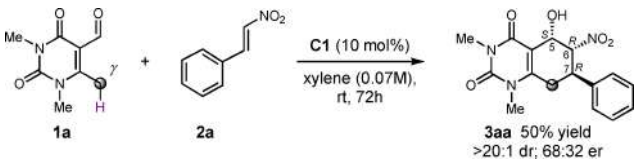

Scheme 3. Model Reaction of the Takemoto's Thiourea-Catalyzed Asymmetric (4+2) Cycloaddition between Uracil Carbaldehyde **1a** and *trans*-*β*-Nitrostyrene (**2a**). Reaction performed under inert atmosphere using **1a** (0.09 mmol), **2a** (1.0 equiv.), and **C1** (10 mol%) in xylene (0.07 M) at rt for 72 h. Yield refers to isolated yield after flash chromatographic purification; the enantiomeric ratio (*er*) was determined by chiral HPLC analysis. Compound **3aa** was obtained as a single isomer. For further details, see the Supp. Info.

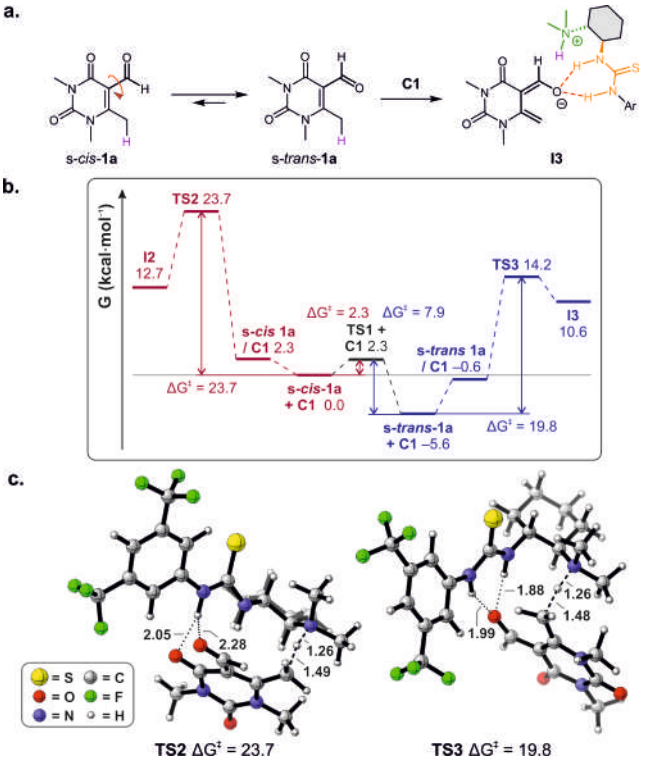

Figure 1. Step 1: Vinylogous dearomative enolization. (a) Overall reaction to dienolate intermediate **I3**. (b) Energetic profile of the deprotonation of s-*cis* **1a** (pink) *vs* s-*trans*-**1a** (blue) by **C1**. (c) Transition states (TSs) of the deprotonation of s-*cis* **1a** (**TS2**) and s-*trans* **1a** (**TS3**). Energies in kcal·mol^{-1}, distances in Angstrom (see the Supp. Info for details).

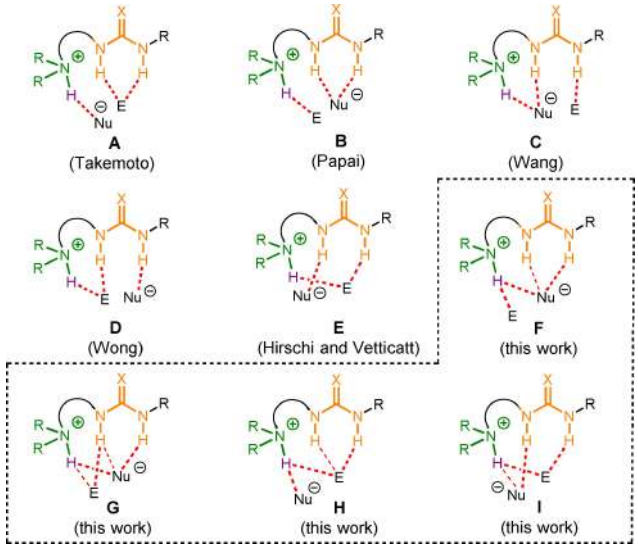

Figure 2. Dual activation modes found operative in the addition of an anionic nucleophile (Nu^-) to a neutral electrophile (E) in the pre-reaction complexes with an amine-thiourea organocatalyst of type **C1**. In the dashed box, new activation modes unveiled in this work with the shorter hydrogen-bonds depicted in bold.

A conformational analysis on uracil carbaldehyde **1a** in the presence of catalyst **C1**, revealed that the s-*trans* conformation is more stable than the corresponding s-*cis* by 5.6 kcal·mol^{-1}, with a very low interconversion barrier (TS1, $\Delta G^{\ddagger}$ 2.3 kcal·mol^{-1}, Figure 1b). The deprotonation steps of both s-*trans* **1a** and s-*cis* **1a** using the Takemoto's catalyst *anti-anti* conformation[18] are endoergonic processes (ΔG_{298} 10.6 kcal·mol^{-1} for s-*trans* **1a** and 12.7 kcal·mol^{-1} for s-*cis* **1a**), but the activation barrier for the deprotonation of s-*trans* **1a** is considerably lower (Figure 1b, $\Delta G^{\ddagger}$ 19.8 kcal·mol^{-1} for s-*trans* **1a** and 23.7 kcal·mol^{-1} for s-*cis* **1a**). Considering both the stability of the starting uracil **1a** conformations and the deprotonation energy barriers, the active intermediate seems to be that deriving from the s-*trans* conformer (**I3** in Figure 1b); thus, all subsequent calculations were conducted using this conformation.

2. Vinylogous Michael Addition Step. The subsequent vinylogous Michael addition step was examined, also capitalizing on the different activation modalities reported so far in the literature for similar tertiary amine/thiourea-catalyzed C–C bond forming reactions (Figure 2).

In particular, modes **A** and **B** refer to those originally proposed by Takemoto[11] and Pápai,[19] respectively, mode **C** was introduced later by Wang,[20] while modes **D** and **E** were recently disclosed by Wong,[21] Hirschi and Vetticatt.[22] These activation modalities differ each other in the hydrogen-bond network established in the pre-reaction complexes between the catalyst and the basic sites in both the nucleophile and electrophile components. Among the number of different pre-reaction complexes examined between the protonated catalyst **C1**, the *ortho*-quinodimethane species generated during the deprotonation of uracil **1a** and the (*E*)-*β*-nitrostyrene **2a**, only four possible approaches were productive for the formation of the new C–C bond (Paths 1–4, Figure 3).

Two of these approaches (Path 1 via mode **B** and Path 2 via mode **A**) would lead to the (*S*)-configuration of the new C7 stereogenic center (observed in the minor enantiomer of **3aa**). The other two approaches would form the new C7 stereogenic center in the observed (*R*)-configuration and are characterized by two novel activation modalities, here called **F** for Path 3 and **G** for Path 4 (Figures 2 and 3a). According to mode **F**, the *ortho*-quinodimethane dienolate is bound

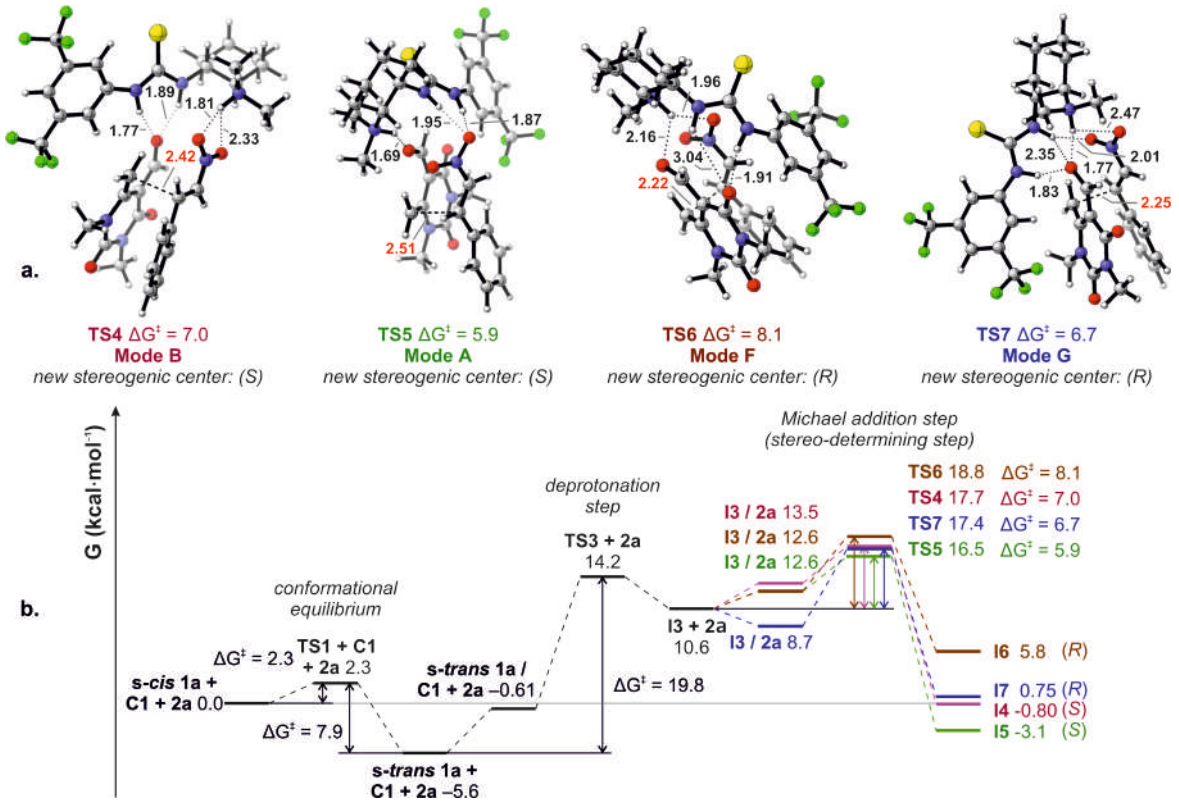

Figure 3. a) Transition states (TSs) in the stereo-defining Michael addition for calculated Paths 1–4. Energies in kcal·mol^{-1}, distances in Angstrom; C–C bond distance in red (see the Supp. Info. for details). (b) Overall reaction profiles (Path 1: pink, Path 2: green, Path 3: brown, Path 4: blue) for the addition of **1a** to **2a** catalyzed by **C1**, up to the Michael addition step. Free-energy profiles at the M06-2X/def2-TZVPP-IEFPCM (toluene)//M06-2X/6–31G(d)-IEFPCM (toluene) level of theory. Energies from single points calculations, corrected using the program GoodVibes (Truhlar's quasi-harmonic approximation).

to both the quaternary ammonium ion moiety and the thiourea H-atoms of **C1**, with hydrogen-bonds involving the enolate oxygen (2.16 Å) and O(C4) oxygen of the uracil ring (1.91 Å), respectively. Concomitantly, the quaternary ammonium ion activates the nitrostyrene electrophile **2a** (1.96 Å). In mode **G**, again the catalyst establishes threefold H-bonding with the *ortho*-quinodimethane dienolate (1.77 Å, 1.83 Å and 2.35 Å), but it involves the enolate oxygen solely. In this case, the electrophile is mainly activated by a hydrogen-bond with the thiourea (2.01 Å), as well as a longer hydrogen-bond with the ammonium salt (2.47 Å). Of note, no activation mode in which each oxygen of the nitro group is bound to a different hydrogen of the thiourea, as originally reported by Takemoto,[11b] was found productive for the Michael reaction. In all cases, the Michael addition is an exergonic reaction, characterized by a rather low activation barrier (~6–8 kcal·mol^{-1}). The four transition states (**TS4--TS7**) identified for this transformation are depicted in Figure 3 (Paths 1–4).

The overall free-energy reaction profiles so far obtained are depicted in Figure 3b, starting from the conformational equilibrium between s-*cis* **1a** and s-*trans* **1a**, passing through the uracil deprotonation to give the *ortho*-quinodimethane dienolate **I3**, the formation of the ternary pre-reaction complex with (*E*)-*β*-nitrostyrene **2a** and up to the Michael addition stereodetermining step. In a previous work, when modelling the cinchona thiourea-catalyzed Michael addition of nitromethane to (*E*)-*β*-nitrostyrene, Grayson considered the pre-reaction complexes to be in rapid equilibrium, so that their relative thermodynamic stabilities did not determine the preferred reaction pathway,[14b,c] according to the Curtin-Hammett principle.[23] These considerations were based on the results obtained by Pápai for the Michael addition of acetylacetone to nitrostyrene, catalyzed by Takemoto's thiourea.[19] The Curtin-Hammett approximations are valid when the rates of isomer interconversion are significantly faster than the rates of product formation. In these papers, the energies involved in pre-reaction complexes formation were assumed to be much smaller than the ones calculated for the C–C bond formation step (~12 kcal·mol^{-1}). In our work though, given that the activation energies for the Michael addition step are significantly lower (~6–8 kcal·mol^{-1}), it is possible that the stereoselectivity is not clearly determined by the Curtin-Hammett principle.

Indeed, in the boundary condition of kinetic quenching, the most stable pre-reaction complex (**I3**/**2a** 8.7 kcal·mol^{-1}; Path 4, blue line, Figure 3b) should determine the stereoselective formation of the new stereogenic center in the observed (*R*)-configuration exclusively. On the other hand, in the boundary condition of the validity of the Curtin-Hammett approximation, the most stable transition state (**I5** −3.1 kcal·mol^{-1}, Path 2, green line, Figure 3b) should favour the sole formation of the (*S*)-configured product. The most convincing scenario here implies that the pre-reaction complexes distribution strongly favours one enantiomer ($\Delta G_{298} = 3.9$ kcal·mol^{-1} > $\Delta G^{\ddagger}_{TS} = 0.8$ kcal·mol^{-1}), but this selectivity is attenuated in the subsequent transition states, and this may rationalize the observed low enantioselective reaction (vide infra).[24]

3. Intramolecular Nitro-Aldol Cyclization Step. To better understand the overall energetics involved in these organocatalyzed transformations, we also modelled the subsequent intramolecular nitro-aldol (Henry) cyclization to the final product **3aa**. Interestingly, calculations remarked an extremely stereoselective cyclization reaction, leading to the 5,6-*cis*-6,7-*trans*-configured diastereoisomer, exclusively, as observed experimentally. The four located transition states (**TS8--TS11**), relative to the Henry ring closure starting from intermediates **I4-I7** are reported in Figure 4a. Transition state **TS8** is characterized by a classic Takemoto's activation mode (mode **A**, Figure 2), where this time the nitronate nucleophile is H-bound to the protonated amine base and the formyl oxygen is H-bonded to the thiourea hydrogen atoms. Transition state **TS9**, instead, features the intricated network of H-bonding of the newly disclosed activation modality **F** (Figure 2) which has been already observed for **TS6**. On the contrary, **TS10** and **TS11** experience two previously undisclosed activation modes, here called mode **H** and **I**, respectively (Figure 2). These **H** and **I** modalities (Figure 4a) entail the uracil electrophile being bound to both the quaternary ammonium moiety and the thiourea group; in the former (mode **H**) the hydrogen bonds engage both the aldehyde oxygen (1.86 Å) and the C4-oxygen of the uracil ring (2.01 Å), while in the latter (mode **I**) only the aldehyde oxygen is involved (1.77 and 2.04 Å). Furthermore, in mode **H**, the nitronate nucleophile is activated solely by the ammonium group (2.28 and 2.55 Å), while in mode **I** the nitronate is bound to both the thiourea (1.89 Å) and to the ammonium salt, by a longer hydrogen-bond (2.38 Å). Looking at the energy profiles of the ring closure reactions depicted in Figure 4b, we notice that three out of four reactions are exergonic transformations (e.g., Paths 2–4; $\Delta G_{298} = \sim -10$–$22$ kcal·mol^{-1}), while Path 1 involving intermediate **I4** is an almost isoergonic reaction ($\Delta G_{298} = \sim 0.5$ kcal·mol^{-1}). By close inspection of the different activation modes and the relative reaction paths of these cyclizations (IRCs, see the Supp. Info. for details), it appears evident that the main difference between Path 1 and the other reaction paths is mainly due to the stabilizing and spontaneous proton transfer from the ammonium moiety to the final alcoholates, due to the proximity of the formyl electrophile to the ammonium acidic site, as appears in modes **F**, **H** and **I**.

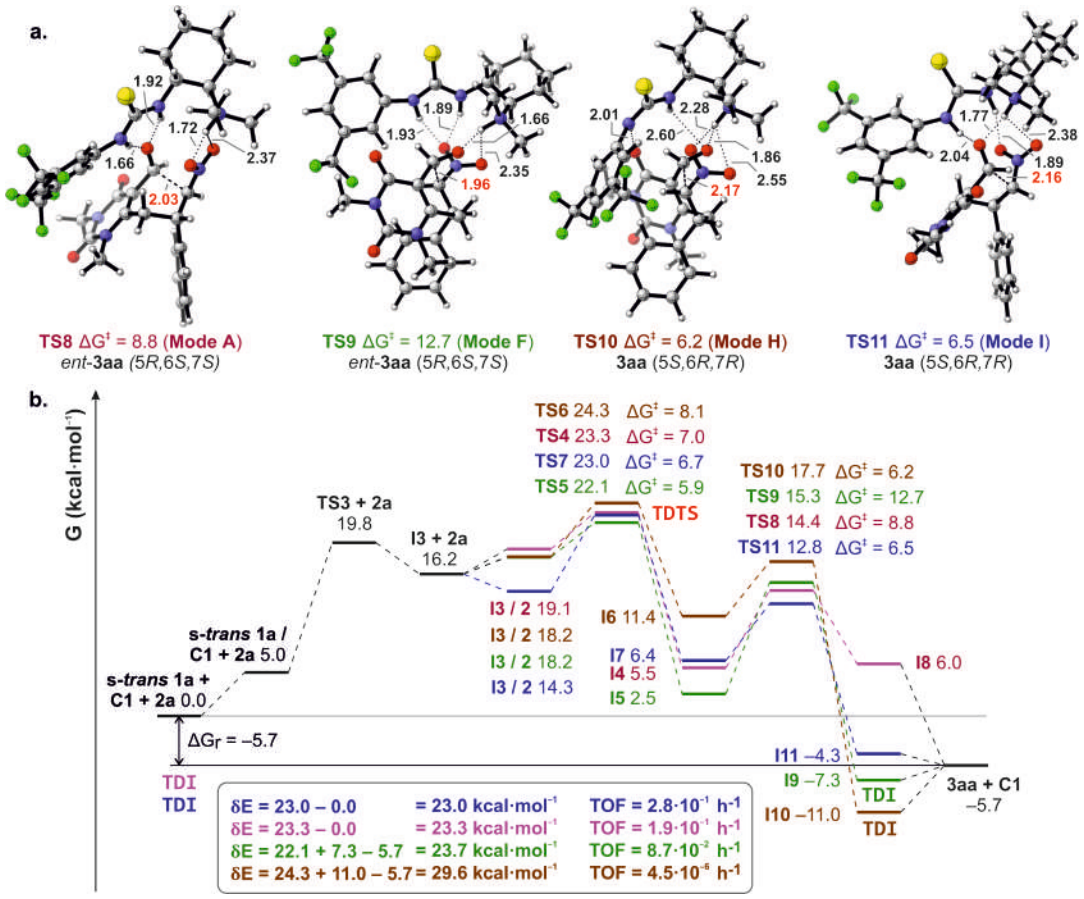

Figure 4. (a) Transition states (**TS**s) in the intramolecular Henry cyclization for calculated Paths 1–4 (Path 1: pink, Path 2: green, Path 3: brown, Path 4: blue). Energies in kcal·mol^{-1}, distances in Angstrom; C–C bond distance in red (see the Supp. Info. for details). (b) Overall reaction profiles for the addition of s-*trans* **1a** to **2a** catalyzed by **C1**, up to the final product **3aa**. Free-energy profiles at the M06-2X/def2-TZVPP-IEFPCM (toluene)//M06-2X/6-31G(d)-IEFPCM (toluene) level of theory. Energies from single points calculations, corrected using the program GoodVibes (Truhlar's quasi-harmonic approximation).

4. Application of the Energetic Span Model. In Figure 4, the complete reaction profiles for the four calculated pathways are reported, by starting from uracil s-*trans*-**1a**, and including the final catalyst decomplexation step to afford the final product **3aa**. By applying the Energetic Span Model proposed by Kozuch and Shaik[7,8] to the overall energetic profile of Figure 4, the TOF-determining transition state (TDTS) matched the C–C bond-forming step of the stereo-determining Michael addition for all the calculated reaction paths. For what concerns the TOF-determining intermediate (TDI), both Path 2 (green) and Path 3 (brown) possess a low-lying TDI located after the TDTS and just before the decomplexation step. On the contrary, the TDIs for both Path 1 (pink) and Path 4 (blue) lie before the TDTS and correspond to the initial step of the related catalytic cycles. This difference in the energy profiles makes the Energetic Span (δE) of Path 1 (23.3 kcal·mol^{-1}) and Path 4 (23.0 kcal mol^{-1}), slightly lower than Path 2 (23.7 kcal·mol^{-1}) and much lower than Path 3 (29.6 kcal·mol^{-1}). Calculation of the turnover frequency (TOF) of the calculated competing catalytic cycle as dictated by the ESM, as well as calculation of the relative kinetic constants using the Eyring equation, show that Path 4 (TOF = 2.8 10^{-1} h^{-1}) is ~3 times faster than Path 2 (TOF = 8.7 10^{-2} h^{-1}) and ~1.5 times faster than the competing Path 1 (TOF = 1.9 10^{-1} h^{-1}).[25] Of note, the difference in Gibbs free energy between the two most favourable reaction paths namely, path 4 *vs* path 1 ($\Delta\Delta G^{\neq}$ = 0.3 kcal·mol^{-1}, *er* = 62:38), is very close to the value observed experimentally ($\Delta\Delta G^{\neq}$ = 0.45 kcal·mol^{-1}, *er* = 68:32), favouring the formation of (5*S*,6*R*,7*R*)-**3aa** via Path 4 over (5*R*,6*S*,7*S*)-*ent*-**3aa** via Path 1. The two competing catalytic cycles (Path 4 *vs* Path 1) for the one pot-four step (4 + 2) cycloaddition between uracil derivative **1a** and nitroalkene **2a** catalyzed by bifunctional thiourea **C1** as calculated in the present study are summarized in Scheme 4.

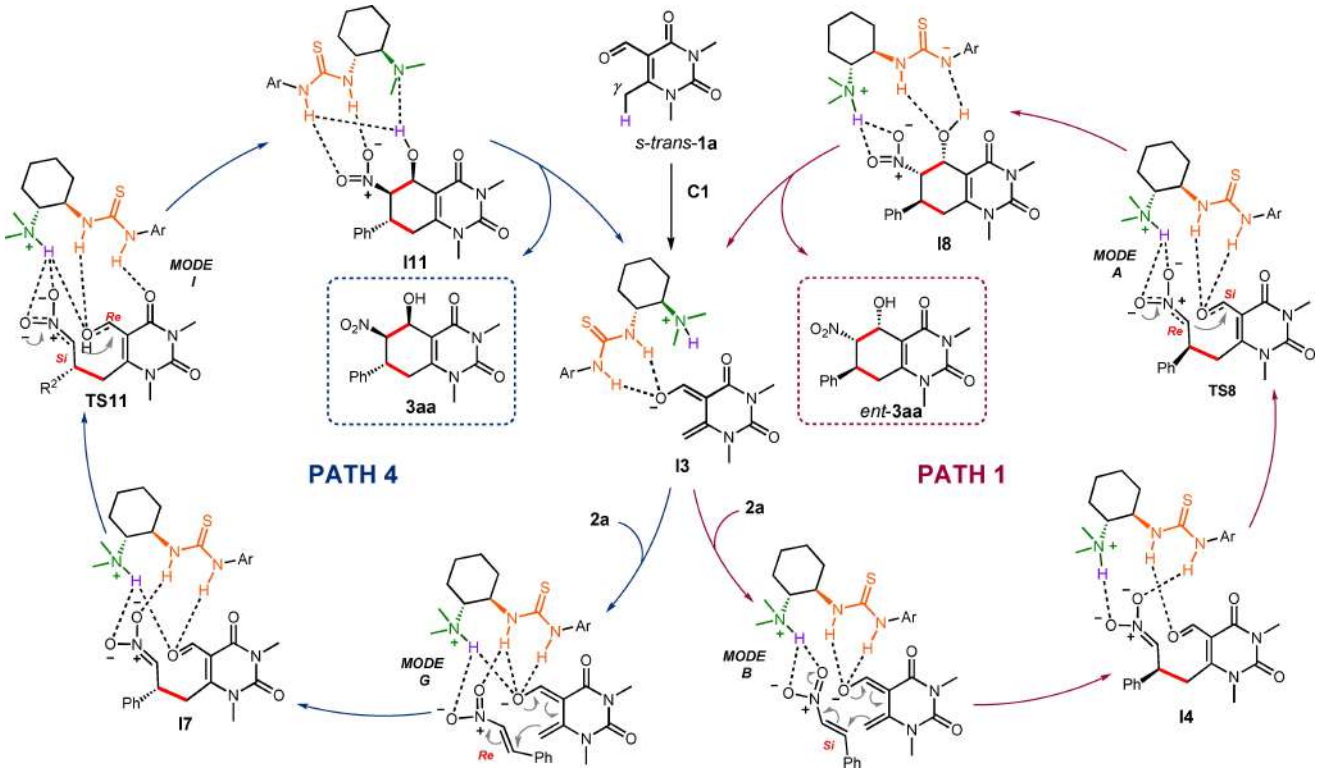

Scheme 4. Calculated competing catalytic pathways in the Takemoto's thiourea-catalyzed asymmetric (4 + 2) cycloaddition between uracil carbaldehyde **1 a** and *trans*-*β*-nitrostyrene (**2 a**).

Conclusions

In conclusion, DFT calculations show that the (4 + 2) cycloaddition of uracil **1 a** to nitrostyrene **2 a** catalyzed by Takemoto's organocatalyst **C1** is characterized by a four-step consecutive cascade including a key stereodetermining Michael addition, followed by a spontaneous and highly diastereoselective intramolecular Henry reaction. The stereoselective formation of the first stereogenic center can be explained either by using a subset of the typical Curtin-Hammett conditions ($\Delta G_{298} > \Delta G^{\ddagger}_{TS}$), or by analyzing the complete catalytic cycle in the framework of the Energetic Span Model (ESM). The energetically most favorable reaction path (Path 4, blue) is characterized by two undisclosed activation modes (mode **G** for the Michael addition and mode **I** for the ring closing step), most probably due to the structure of the vinylogous uracil-based substrate **1 a**. On the other hand, the competing reaction path (Path 1, pink) leading to *ent*-**3 aa**, is characterized by known activation modalities such as mode **B** for the Michael addition, and Mode **A** for the Henry cyclization.

The application of the ESM to the complete, calculated energetic profile of the reaction, confirmed the experimental data by framing a cascade reaction in which four competing catalytic cycles are operative leading to the formation of the chiral product whose calculated enantiomeric ratio well matched the experimental one. These results highlight once more the usefulness of the ESM in the evaluation of the efficiency of catalytic cycles when a complete energy profile of the process is provided, paving the way for a more general and robust application of the method to novel challenging organocatalytic transformations, involving complex substrates or highly reactive intermediates.

Finally, the efficiency of Takemoto's catalyst **C1** in promoting the stereoselective Michael addition to nitroalkenes, and the subsequent Henry cyclization, using unique pro-nucleophiles such as *N*-protected 6-methyluracil-5-carbaldehydes, emphasizes once more the great versatility and generality of this family of bifunctional organocatalysts, able to adapt the hydrogen-bond network to profitably activate reaction partners of different natures.

Experimental Section

Computational Details

Calculations were performed using Gaussian 16, Revision C.01.[26] Geometries were optimized using the M06-2X density functional[27] and the 6-31G(d) basis set within the IEFPCM model (solvent = toluene)[28] and further confirmed to be sta-

tionary points on the potential energy surface by frequency calculations. Transition states were confirmed to join the correct minimum energy structures by IRC calculations. Single point energies were calculated using the M06-2X density functional and def2-TZVPP basis set within the IEFPCM model (solvent = toluene)[28] and corrected using the program GoodVibes (Truhlar's quasi-harmonic approximation).[29] Molecules possessing conformational mobility were first optimized using molecular mechanics (MMFF94 force field); all the conformers within a 10 kcal·mol^{-1} window were then re-optimized using DFT and only the lowest energy conformer was used in all subsequent calculations. All molecule illustrations were made using with CYLView.[30] Energetic Span calculations were made using the program AUTOF (Excel version).[25]

Synthesis of (5S,6R,7R)-Configured Fused Uracil (3 aa)

In a round-bottomed flask equipped with a magnetic steer bar and kept under nitrogen atmosphere, 1,3,6-trimethyl-2,4-dioxo-1,2,3,4-tetrahydropyrimidine-5-carbaldehyde **1 a** (16.2 mg, 0.089 mmol, 1 equiv.) and *trans-β*-nitrostyrene **2 a** (13.3 mg, 0.089 mmol, 1 equiv.) were dissolved in xylene (1.25 mL) at 25 °C. Catalyst (*R,R*)-**C1** (3.7 mg, 0.009 mmol, 0.1 equiv.) was then added, and the resulting reaction was stirred at 25 °C and monitored by TLC. After 72 h, the heterogeneous mixture was directly subjected to flash chromatography on silica gel (petroleum ether/ethyl acetate 3:7) to afford **3 aa** (14.7 mg, 50% yield) as a pale-yellow solid. The enantiomeric ratio of the product was determined to be 68:32 by HPLC analysis on a Chiralcel OD–H column (eluent: 60:40 Hexane/EtOH; flow rate 1.0 mL/min, λ = 254 nm. τ_{Major} = 24.3 min, τ_{Minor} = 35.4 min).

Acknowledgements

Prof. S. Kozuch and Prof. M. N. Grayson are gratefully acknowledged for the helpful discussions. We also thank Dr. L. Marzocchi for proofreading the manuscript. University of Parma and University of Bologna are acknowledged for the financial support. Open Access Funding provided by Universita degli Studi di Bologna within the CRUI-CARE Agreement.

References

[1] For a recent, comprehensive review on definitions and applications of organocascade reactions, see: E. Massolo, M. Benaglia, *Physical Sciences Reviews* **2021**, 20180096.

[2] a) C. Grondal, M. Jeanty, D. Enders, *Nat. Chem.* **2010**, *2*, 167–178; b) C. Curti, L. Battistini, A. Sartori, F. Zanardi, *Chem. Rev.* **2020**, *120*, 2448–2612.

[3] J. L. Segura, N. Martín, *Chem. Rev.* **1999**, *99*, 3199–3246.

[4] A. Przydacz, A. Skrzyńska, Ł. Albrecht, *Angew. Chem. Int. Ed.* **2019**, *58*, 63–73; *Angew. Chem.* **2019**, *131*, 64–75.

[5] F. Braak ter, H. Elferink, K. J. Houthuijs, J. Oomens, J. Martens, T. J. Boltje, *Acc. Chem. Res.* **2022**, *55*, 1669–1679.

[6] a) P. H.-Y. Cheong, C. Y. Legault, J. M. Um, *Chem. Rev.* **2011**, *111*, 5042–5137; b) Q. Peng, R. S. Acc, *Chem. Res.* **2016**, *49*, 1042–1051; c) S. Ahn, M. Hong, M. Sundararajan, D. H. Ess, M.-H. Baik, *Chem. Rev.* **2019**, *119*, 6509–6560.

[7] a) S. Kozuch, S. Shaik, *Acc. Chem. Res.* **2011**, *44*, 101–110; b) S. Kozuch, *WIREs Comput. Mol. Sci.* **2012**, *2*, 795–815; c) S. Kozuch, J. M. L. Martin, *ACS Catal.* **2012**, *2*, 2787–2794; d) E. Solel, N. Tarannam, S. Kozuch, *Chem. Commun.* **2019**, *55*, 5306–5322.

[8] According to Kozuch's model, the energetic span δE of a computed catalytic cycle can be calculated as follows: $\delta E = T_{TDTS} - I_{TDI}$ if the TDTS follows the TDI; $\delta E = T_{TDTS} - I_{TDI} + \Delta G_{rx}$ if the TDTS precedes the TDI; where ΔG_{rx} is the Gibbs free energy of the reaction.

[9] For recent, selected applications of the Energetic Span Model to organocatalyzed reactions, see: a) Y. Reddi, R. B. Sunoj, *ACS Catal.* **2017**, *7*, 530–537; b) R. Maji, P. A. Champagne, K. N. Houk, S. E. Wheeler, *ACS Catal.* **2017**, *7*, 7332–7339; c) B. Bhaskararao, R. B. Sunoj, *Chem. Sci.* **2018**, *9*, 8738–8747; d) R. Rowshanpour, M. Gravel, T. Dudding, *J. Org. Chem.* **2022**, *87*, 16785–16793.

[10] E. Marcantonio, C. Curti, L. Battistini, A. Sartori, L. Cardinale, G. Pelosi, F. Zanardi, *Adv. Synth. Catal.* **2021**, *363*, 2625–2633.

[11] a) T. Okino, Y. Hoashi, Y. Takemoto, *J. Am. Chem. Soc.* **2003**, *125*, 12672–12673; b) T. Okino, Y. Hoashi, T. Furukawa, X. Xu, Y. Takemoto, *J. Am. Chem. Soc.* **2005**, *127*, 119–125.

[12] The use of chiral tertiary amine-thiourea organocatalysts to promote asymmetric cascade transformations for the generation of complex molecule, has recently been reviewed: S. Gandi, V. Sivadas, B. Baire, *Eur. J. Org. Chem.* **2021**, 220–234.

[13] C. Curti, G. Rassu, M. Lombardo, V. Zambrano, L. Pinna, L. Battistini, A. Sartori, G. Pelosi, F. Zanardi, *Angew. Chem. Int. Ed.* **2020**, *59*, 20055–20064; *Angew. Chem.* **2020**, *132*, 20230–20239.

[14] a) J. R. Pliego Jr, *Phys. Chem. Chem. Phys.* **2020**, *22*, 11529–11536; b) M. N. Grayson, K. N. Houk, *J. Am. Chem. Soc.* **2016**, *138*, 9041–9044; c) M. N. Grayson, K. N. Houk, *J. Am. Chem. Soc.* **2016**, *138*, 1170–1173.

[15] Selected examples: a) Y.-J. Tsou, N. Sthishkumar, I.-T. Chen, T.-A. Lee, H.-T. Chen, J.-L. Han, *J. Org. Chem.* **2022**, *87*, 2520–2531; b) B. Tan, Y. Lu, X. Zeng, P. J. Chua, G. Zhong, *Org. Lett.* **2010**, *12*, 2682–2685.

[16] For a related example see: F. Esteban, V. Cieślik, E. M. Arpa, A. Guerrero-Corella, S. Díaz-Tendero, J. Perles, J. A. Fernández-Salas, A. Fraile, J. Alemán, *ACS Catal.* **2018**, *8*, 1884–1890.

[17] A. M. F. Phillips, M. H. G. Prechtl, A. J. L. Pombeiro, *Catalysts* **2021**, *11*, 569–621.

[18] A. Capobianco, S. Mennino, A. Lattanzi, *Catal. Sci. Technol.* **2020**, *10*, 1422–1430.

[19] A. Hamza, G. Schubert, T. Soós, I. Pápai, *J. Am. Chem. Soc.* **2006**, *128*, 13151–13160.
[20] J.-L. Zhu, Y. Zhang, C. Liu, A.-M. Zheng, W. Wang, *J. Org. Chem.* **2012**, *77*, 9813–9825.
[21] J. Guo, M. W. Wong, *J. Org. Chem.* **2017**, *82*, 4362–4368.
[22] J. A. Izzo, Y. Myshchuk, J. S. Hirschi, M. J. Vetticatt, *Org. Biomol. Chem.* **2019**, *17*, 3934–3939.
[23] J. I. Seeman, *Chem. Rev.* **1983**, *83*, 83–134.
[24] M. Roth, D. Wolfgang, B. Giese, *Tetrahedron Lett.* **1996**, *37*, 351–354.
[25] ESM calculations were made using the free program AUTOF (Excel version). See reference 7b and https://www.bgu.ac.il/~kozuch/software.html.
[26] Gaussian 16, Revision C.01, M. J. Frisch, G. W. Trucks, H. B. Schlegel, G. E. Scuseria, M. A. Robb, J. R. Cheeseman, G. Scalmani, V. Barone, G. A. Petersson, H. Nakatsuji, X. Li, M. Caricato, A. V. Marenich, J. Bloino, B. G. Janesko, R. Gomperts, B. Mennucci, H. P. Hratchian, J. V. Ortiz, A. F. Izmaylov, J. L. Sonnenberg, D. Williams-Young, F. Ding, F. Lipparini, F. Egidi, J. Goings, B. Peng, A. Petrone, T. Henderson, D. Ranasinghe, V. G. Zakrzewski, J. Gao, N. Rega, G. Zheng, W. Liang, M. Hada, M. Ehara, K. Toyota, R. Fukuda, J. Hasegawa, M. Ishida, T. Nakajima, Y. Honda, O. Kitao, H. Nakai, T. Vreven, K. Throssell, J. A. Montgomery Jr., J. E. Peralta, F. Ogliaro, M. J. Bearpark, J. J. Heyd, E. N. Brothers, K. N. Kudin, V. N. Staroverov, T. A. Keith, R. Kobayashi, J. Normand, K. Raghavachari, A. P. Rendell, J. C. Burant, S. S. Iyengar, J. Tomasi, M. Cossi, J. M. Millam, M. Klene, C. Adamo, R. Cammi, J. W. Ochterski, R. L. Martin, K. Morokuma, O. Farkas, J. B. Foresman, D. J. Fox, Gaussian, Inc., Wallingford CT (2016).
[27] Y. Zhao, D. Truhlar, *Theor. Chem. Acc.* **2008**, *120*, 215.
[28] J. Tomasi, B. Mennucci, R. Cammi, *Chem. Rev.* **2005**, *105*, 2999.
[29] G. Luchini, J. V. Alegre-Requena, I. Funes-Ardoiz, R. S. Paton, *F1000Research* **2020**, *9*, 291, https://github.com/patonlab/GoodVibes.
[30] C. Y. Legault, CYLView, Université de Sherbrooke: Sherbrooke, Quebec, Canada, **2009**, http://www.cylview.org.